Title

Experimental evaluation of the resolution and quantitative accuracy of temperature-modulated fluorescence tomography.

Journal

Applied Optics, 56(3)

ISSN

1559-128X

Authors

Kwong, Tiffany C

Nouizi, Farouk

Lin, Yuting

et al.

Publication Date

2017-01-20

DOI

10.1364/ao.56.000521

Peer reviewed

Published in final edited form as:

Appl Opt. 2017 January 20; 56(3): 521–529. doi:10.1364/AO.56.000521.

Experimental evaluation of the resolution and quantitative accuracy of temperature-modulated fluorescence tomography

TIFFANY C. KWONG[1,*], **FAROUK NOUIZI**[1], **YUTING LIN**[1,2], **JAEDU CHO**[1], **YUE ZHU**[3], **UMA SAMPATHKUMARAN**[3], **GULTEKIN GULSEN**[1]

[1]Tu and Yuen Center for Functional Onco-Imaging, Department of Radiological Sciences, University of California, Irvine, California 92697, USA

[2]Department of Radiation Oncology, Massachusetts General Hospital and Harvard Medical School, Boston, Massachusetts 02144, USA

[3]InnoSense LLC, Torrance, California 90505, USA

Abstract

Previously, we reported on the spatial resolution and quantitative accuracy of temperature-modulated fluorescence tomography (TM-FT) using simulation studies. TM-FT is a novel fully integrated multimodality imaging technique that combines fluorescence diffuse optical tomography (FT) with focused ultrasound. Utilizing unique thermo-reversible fluorescent nanocapsules (ThermoDots), TM-FT provides high-resolution cross-sectional fluorescence images in thick tissue (up to 6 cm). Focused ultrasound and temperature-sensitive ThermoDots are combined to provide accurate localization of these fluorescent probes and *functional a priori* information to constrain the conventional FT reconstruction algorithm. Our previous simulation studies evaluated the performance of TM-FT using synthetic phantoms with multiple fluorescence targets of various sizes located at different depths. In this follow-up work, we perform experimental studies to evaluate the performance of this hybrid imaging system, in particular, the effect of size, depth, and concentration of the fluorescence target. While FT alone is unable to accurately locate and resolve the fluorophore target in many cases, TM-FT is able to resolve the size and concentration of the ThermoDots within a thick turbid medium with high accuracy for all cases. The maximum error in the recovered ThermoDots concentration and target sizes with TM-FT are 12% and 25%, respectively.

Keywords

(170.0110) Imaging systems; (170.0170) Medical optics and biotechnology; (170.3880) Medical and biological imaging; (110.6955) Tomographic imaging; (110.7050) Turbid media; (260.2510) Fluorescence

[*]Corresponding author: tckwong@uci.edu.

1. INTRODUCTION

Fluorescence diffuse optical tomography (FT) has become increasingly popular as a safe and inexpensive method that can noninvasively reconstruct the distribution of an exogenous fluorescent contrast agent *in vivo* [1]. FT has high signal-tobackground contrast and uses fluorescent probes that can be engineered to provide molecular and cellular information for a number of applications, including diagnosis as well as monitoring treatment response for a variety of diseases from rheumatoid arthritis to cancer [1–4]. Indeed, fluorescence imaging has become a key tool in preclinical imaging [1].

However, high scattering in biological tissue causes poor photon penetration depth, and remains a major obstacle of FT imaging in thick tissue. Combined with the fact that the FT inverse problem is strongly ill-posed and underdetermined, high tissue scattering makes it difficult to recover the distribution of the fluorescent contrast agent. This results in poor spatial resolution and low quantitative accuracy for FT, especially in deep tissue. To overcome this obstacle, multimodality techniques that incorporate structural information provided by anatomical imaging modalities, such as *x*-ray CT, MRI, and ultrasound, have been developed [5–8]. Accordingly, *structural a priori* information obtained by an anatomical imaging modality is used to guide and constrain the optical image reconstruction algorithm and has been shown to significantly improve the quantitative accuracy of FT [5–7,9]. Nevertheless, errors can still occur when the structural boundaries provided by the anatomical imaging modality do not exactly coincide with the true fluorescent distribution [10].

Instead of assuming the fluorophore distribution is confined homogeneously within the structural boundary identified by the separate anatomical imaging modality, an ideal method would be directly mapping the fluorophore distribution to provide *functional a priori* information. For this purpose, focused ultrasound has recently been used in combination with fluorescence tomography [11,12]. In this approach, focused ultrasound is used to modulate the temperature of the medium with high spatial resolution to directly map the position of temperature-sensitive fluorescent contrast agents as a *functional a priori* information. This true multimodality imaging technique called “temperature-modulated fluorescence tomography” (TM-FT) achieves remarkable high spatial resolution and quantitatively accurate images of the thermo-sensitive fluorophores in deep tissue (≤6 cm) [12,13]. The sensitivity of this technique relies on the responsiveness of the activatable thermo-reversible fluorescent probes we call “ThermoDots.” The ThermoDots are based on recent reports of thermo-sensitive fluorescent contrast agents made from Indocyanine green (ICG) loaded Pluronic-F127 polymeric micelles [14,15]. The thermo-responsiveness of the ThermoDots is based on the temperature-dependent hydrophobic/hydrophilic property of the Pluronic polymer micelles. In summary, an increase in temperature induces a variation in the solvent polarity, resulting in an ICG fluorescence signal and lifetime change [13]. Focused ultrasound is used to provide localized heating of the tissue with high resolution by focusing the ultrasound into a small focal zone (~1.33 mm) to heat the medium approximately 4°C. This sudden increase in temperature changes the quantum efficiency of the agents, leading to an increase in the emitted fluorescent light intensity. To locate the ThermoDots, TM-FT utilizes this change in the emitted fluorescence signal, which only occurs when they are

located within the focal zone of the focused ultrasound. Consequently, TM-FT is able to overcome the inherently poor spatial resolution of conventional FT as the resolution of TM-FT is dependent on the size of the focal spot of the focused ultrasound.

Previously, we evaluated the resolution and quantitative accuracy of TM-FT with simulation studies [16]. Recently, we have also presented a faster and improved scanning method that reduces the data acquisition time drastically [10]. In this approach, the focused ultrasound transducer is moved continuously while the fluorescence signal is monitored as opposed to the slow step- and-shoot approach we had initially employed [12]. In this follow-up study, we investigate the performance of our fast TM-FT system with an extensive experimental phantom study using our new scanning method. In the first part of this study, the linearity of the system response is tested using inclusions filled with various dilutions of the activatable and thermo-reversible ThermoDots. Next, the depth and size dependence of the fluorescent inclusion on the recovered ThermoDots concentration is evaluated for TM-FT and compared to conventional FT. Finally, the spatial resolution limit of the system is studied. In all cases, utilization of the focused ultrasound *functional a priori* information from TM-FT resulted in a significant improvement in the spatial resolution and quantitative accuracy compared to conventional FT.

2. METHODS

A. Instrumentation

All experiments were performed with a custom-built system developed for TM-FT [12]. This system integrated focused ultrasound with a conventional frequency-domain FT system. The FT system uses a 785 nm laser diode (300 mW, Thorlabs, USA) to illuminate the object under investigation in a transillumination mode. A fiber optic switch delivers the laser light to one of six source optical fibers (1 mm). A network analyzer (Agilent Technologies, USA) is utilized to simultaneously provide RF modulation (100 MHz) for the laser diode while also measuring the amplitude of the detected signal. The transmitted light is collected by one of six fiber bundles (6 mm) and passes through a series of lens (Newport Corporation, USA) and bandpass filters (830 nm, MK Photonics, *USA*) to eliminate excitation light. A photomultiplier tube (PMT) (R7400U-20, Hamamatsu, Japan) is used to detect the fluorescence signal. The signal is then amplified by an RF amplifier before being recorded by the network analyzer. For TM-FT, the focused ultrasound is incorporated into the FT system. A function generator (PTS 500, Programmed Test Sources, Inc., USA) generates a 1.0 MHz signal, which is amplified by a power amplifier (200L, Amplifier Research, Inc., USA) before delivery to the focused ultrasound transducer (H102, Sonic Concepts, Inc., USA). The focal spot of this transducer (~1.33 mm in diameter and 10 mm in length) is located 60 mm below the transducer; see Fig. 1(a). The transducer is mounted on two computer-controlled automatic translational stages in the x–y plane. A third manual translational stage allows height adjustments for the transducer above the phantom. Both the transducer and the optical interface that holds the fibers together with the phantom are immersed in water.

The focused ultrasound scanning procedure was fully automated using LabVIEW (National Instruments, USA) covering a 50 mm × 25 mm area, as shown in Fig. 1(b). This procedure

consists of two *x*-scans, as indicated by the dashed blue lines, and two y-scans, as indicated by the dashed red lines, with one scan moving in a forward direction and the other scan moving in the reverse direction. The distance between each scanning line is 1.35 mm, nearly the diameter of the focal spot of the transducer, in both *x* and *y* directions. To avoid the effect of heat diffusion from adjacent lines, a jumping pattern is utilized instead of scanning lines in a consecutive fashion. During these scans, the transducer is turned on continuously while the network analyzer records the fluorescence data collected from the source/detector pair with the highest signal-to-noise ratio (SNR). To prevent the effect of heat diffusion from the previously scanned points in the line, the transducer moves at 4.16 mm/s. For a 50 mm line scan, the network analyzer acquires 200 measurements, resulting in a sampling rate of one measurement per 0.25 mm. A filtering window of five data points wide, which roughly corresponded to the size of the focal spot (~1.33 mm) of the transducer is used to smoothen the measured signals. The full width at half-maximum (FWHM) is used as a threshold to create a binary map of the position of the ThermoDots with high spatial resolution. This binary map is used as *functional a priori* to constrain the reconstruction algorithm. A more detailed explanation of the focused ultrasound continuous scanning method is described in Nouizi *et al.* [10].

B. Optical Image Reconstruction Algorithm

Since the quantum efficiency of the ThermoDots is temperature dependent, the coupled diffusion equation at the emission wavelength is altered to account for this dependence on temperature:

$$\begin{cases} -\nabla\left[D_x \nabla\ \Phi_x\right] - \left[\mu_{af} + \mu_{ax}\right] \Phi_x\ =\ -\ q_0, \\ -\nabla\left[D_m \nabla\ \Phi_m\ [\eta(T)]\right] - \mu_{am}\ \Phi_m\ [\eta(T)] =\ -\ \Phi_x\ \eta(T)\mu_{af}, \end{cases} \tag{1}$$

where $\eta(T)$ denotes the temperature-dependent fluorescence quantum yield, and q_0 is the isotropic excitation light source. For the following variables, the subscripts x and m represent the excitation and emission wavelengths, respectively. $\mathbf{\Phi}$(W mm^{-2}) is the photon density, and D describes the diffusion coefficient, $D = 1/3\left(\mu_a + \mu'_s\right)$. The absorption and reduced scattering coefficients of the medium are represented by μ_a and μ'_s, respectively. μ_{af} is the absorption coefficient of the fluorophore and is directly related to its concentration. The synthetic fluorescence signal for the source (s) and detector (d), $S_{s,d}(s, d = 1; 2; \ldots, 6)$, are obtained by solving the coupled diffusion Eq. (1) with the finite element method using a mesh that consists of $N = 6034$ nodes and 11,775 triangular elements.

The absorption coefficient of the fluorescence map, μ_{af}, is recovered by iteratively minimizing the quadratic error between these synthetic signals and the fluorescence ones, $F_{s,d}$, measured on the surface of the phantom. The update to the absorption coefficient of fluorescence, $\Delta\mu_{af}$, is obtained using the Levenberg–Marquardt minimization algorithm after incorporating the binary mask provided by TM-FT as soft *a priori* [17,18]:

$$\Delta\mu_{af} = \left(J^T J + L^T L\right)^{-1} J^T \left(F_{s,d} - S_{s,d}\right)^2, \tag{2}$$

where J represents the Jacobian matrix ($M \times N$), with $M = 36$ being the number of measurements. λ is the inversion regularization factor. L ($N \times N$) is the Laplacian-type *a priori* matrix used to incorporate the binary mask and constrain the reconstruction process. The value of L for a couple of nodes i and j is given by

$$L_{i,j} = \begin{cases} 0 & i, j \text{ in different regions,} \\ -1/N_r & i, j \text{ in the same region,} \\ 1 & i = j, \end{cases} \tag{3}$$

with N_r being the number of nodes in a given region. More details on this method have been published previously [10,16,18].

C. ThermoDots

The ThermoDots are prepared by our industrial collaborator, InnoSense LLC (USA) and consist of ICG encapsulated in Pluronic-F127 polymeric micelles. The ThermoDots are characterized to determine their thermo-responsiveness and active temperature range. For these phantom studies, the ThermoDots were optimized to perform at room temperature (20°C) for convenience and measures a 23 dBm (~15×) increase in the signal amplitude between 20°C and 24°C. The phantom experiments are performed at 20°C and the focused ultrasound is set to heat the medium by 4°C at its focal spot to maximize the fluorescence signal change. Details on ThermoDots preparation and characterization can be found in Kwong *et al.* [19].

D. Phantom Studies

All experiments carried out in this study are performed using a 100 mm × 40 mm × 100 mm phantom-mimicking biological tissue. The phantoms are prepared using intralipid (0.5%) and India ink (Winsor and Newton, UK) to respectively simulate the tissue scattering and absorption properties. The absorption and reduced scattering of the phantom are the same for both excitation and emission wavelengths and set to $\mu_a = 0.008$ mm^{-1} and $\mu'_s = 0.86$ mn^{-1}, respectively.

The inclusions are made from optically transparent glass tubes of varying diameters cut down to 10 mm in length. For the first set of experiments, a 3 mm diameter tube is filled with various concentrations of the ThermoDots to measure the linearity of the system. To investigate the size dependence, tubes with different diameters are utilized (5, 4, 3, and 2 mm) and filled with an 837 nM ThermoDots solution. Following that, a single 3 mm diameter inclusion at the same concentration is positioned at various depths to explore the depth dependence. Finally, two identical 3 mm diameter inclusions are positioned in the center with different separations to evaluate the spatial resolution and performance of TM-FT. In all cases, the axis of the tube is aligned with the focused ultrasound column in the z direction and centered in line with the optical fiber plane.

3. RESULTS AND DISCUSSION

A. Phantom Study 1: System Response Linearity

For this study, a single 3 mm glass tube is embedded in the tissue-mimicking phantom as described previously in Fig. 1. The tube is consecutively filled with different concentrations of the ThermoDots to investigate the performance of TMFT to accurately recover each concentration. Dilutions are performed on the ThermoDots solution (100%, 90%, 60%, and 40%) to achieve four different concentrations: 837, 782, 516, and 358 nM.

Figure 2 shows the ThermoDots concentration images reconstructed without and with the *functional a priori* information provided by the focused ultrasound. As seen from this figure, the ThermoDots concentration is accurately recovered with TM-FT and has less than a 4% error for all four cases compared to conventional FT, which greatly underestimates all four concentrations. In addition, although the size of the inclusions is overestimated using conventional FT, the addition of the focused ultrasound *functional a priori* information of TM-FT considerably improves the recovered size of the inclusion. The results of the concentration and inclusion size recovered from TM-FT and conventional FT are summarized in Table 1.

Figure 3 shows that the recovered ThermoDots concentration is linear with respect to the true concentration for both TM-FT and FT alone. The correlation coefficient for the TM-FT and stand-alone FT fitted curves is 0.998 and 0.863, respectively. Although, the recovered ThermoDots concentration is severely underestimated with FT alone, the accuracy of the recovered ThermoDots concentration is greatly improved for all cases when the focused ultrasound *functional a priori* information is utilized.

Indeed, the recovered concentration accuracy directly depends on the spatial resolution of the system. For the conventional FT, the spatial resolution in the y direction is expected to be lower than the x direction due the transillumination confuguration of the system. This can be seen by comparing the recovered size of the inclusion in orthogonal directions. For all four cases, the recovered object size in conventional FT images is significantly larger in the y direction (~6 ×) compared to the x direction (~1.6 ×). Accordingly, as the ThermoDots fluorescent signal is attributed to a larger area, this resulted in a large percent error in the recovered concentration(≥ 89%).

TM-FT uses the focused ultrasound scan to create a binary map of the ThermoDots distribution with high spatial resolution. With the addition of this *functional a priori* data, TM-FT is able to recover quantitatively accurate concentration values for the ThermoDots with less than 4% error. TM-FT is not affected by the source–detector geometry as the spatial resolution of TM-FT is primarily determined by the focused ultrasound. The error in the recovered size of the ThermoDots is even in both the x and y directions and varies between 0–25% in the recovered size of the object for the four concentrations.

A slight trend is observed with the higher concentrations of the ThermoDots (Case 1 and 2) having a smaller percent error than Case 3 and 4. This is reasonable as the lower

concentrations would result in a lower fluorescent signal and lead to a lower SNR, which makes recovering the concentration more challenging.

B. Phantom Study 2: Size Dependence

The performance of TM-FT in recovering inclusions of different sizes is studied using four different sized inclusions: 5, 4, 3, and 2 mm. The inclusions are positioned equidistance between the source and the detector fibers, as shown in Fig. 1. The recovered absorption maps of the ThermoDots obtained with TM-FT and conventional FT are presented in Fig. 4.

The effect of inclusion size on the accuracy of the recovered fluorophore absorption can be seen in Table 2. For conventional FT, the size of inclusion is overestimated in both x and y directions while the ThermoDots absorption is greatly underestimated for all four sizes. The error in the recovered absorption of the ThermoDots is over 90% for all four cases. An increase in the percent error of the recovered size and absorption of the ThermoDots is observed as the size of the object decreases. As expected, the accuracy of the recovered ThermoDots absorption is higher when the inclusion is of larger size, due to the higher SNR. However, the addition of the *functional a priori* information using TM-FT considerably improves the size and quantitative accuracy. For all four cases, the recovered size of the ThermoDots inclusion is off by only ±0.25 mm and is not size dependent. With TMFT, there is only a slight size dependence as the recovered concentrations for Cases 5–7 (diameters of 5, 4, and 3 mm, respectively) are close to the true value and have similar error.

The percent error in the recovered absorption for the 2 mm case increases twofold but is still acceptable at 12%. Overall, the maximum error in the recovered size and absorption of the ThermoDots inclusion using TM-FT is 12.5% and 12% error, respectively, indicating that the size dependence of TM-FT is minimal as long as the object is equal to or larger than the focused ultrasound focal spot.

C. Phantom Study 3: Depth Dependence

To study the effect that the position of the inclusion has on the recovered fluorescence absorption, a 3 mm inclusion is filled with the same ThermoDots concentration and positioned at four different distances from detector 3: 20, 15, 10, and 5 mm, as shown in the left column of Fig. 5. The ThermoDots fluorescence absorption maps are reconstructed with and without *functional a priori* information and compared in Fig. 5. The results of all four cases are summarized in Table 3.

When the inclusion is positioned equidistance from source 3 and detector 3, the recovered ThermoDots fluorescence absorption coefficient is 0.0182 mm^{-1}, yielding an 8.9% error for TM-FT. When the inclusion is moved closer to the detectors at 15, 10, and 5 mm away, the fluorescence absorption coefficient is recovered with 0.8%, 6%, and 10.2% errors, respectively. Contrarily, for conventional FT without the use of *a priori* information, the fluorescence absorption coefficient is recovered with over 90% error for these cases (9–11). Meanwhile, when the inclusion is positioned only 5 mm away from detector 3, the FT reconstruction program failed to separate the inclusion from the detector.

The reconstructed fluorescence absorption is expected to depend on the location of the inclusion due to the transillumination configuration of the system [20]. The accuracy of the recovered ThermoDots absorption is dependent on the sensitivity, which is highest in the center of the phantom when the inclusion lies within multiple source–detector pair paths. This is seen in the conventional FT cases as the error in the recovered concentration increases as the inclusion moves away from center toward the edge of the phantom. Conventional FT is unable to resolve the inclusion, positioned 5 mm away from the detector, as it is located in an area of low sensitivity.

However, TM-FT utilizes the *functional a priori* information from the focused ultrasound to establish the position of the fluorescence during the initialization of the reconstruction algorithm and is not affected by the optical source–detector configuration. As seen in Fig. 5, TM-FT resolves all inclusions successfully, including the one located at the depth of 5 mm and recovers the ThermoDots fluorescence absorption with a maximum of 10.2% error for all depths.

D. Phantom Study 4: Spatial Resolution

In the last study, the spatial resolution of the TM-FT system is investigated using multiple inclusions. In this study, two identical 3 mm inclusions filled with the same ThermoDots concentration are placed at decreasing distances from each other in order to find the resolution limit of our system, as shown in Fig. 6. Four cases are studied: 1.4, 3, 6.3, and 9 mm separation between the edges of the two objects. Figure 7 shows the ThermoDots fluorescence absorption maps reconstructed with TM-FT and conventional FT.

The inherent limited spatial resolution of FT is clearly seen in the recovered ThermoDots fluorescence absorption maps in Fig. 7. Conventional FT is only able to resolve the two objects for the largest separation of 9 mm. The two inclusions are overestimated in size and severely underestimated in the recovered ThermoDots fluorescence absorption with over an 87% error. Excluding this case, FT is unable to resolve the two inclusions as separate entities and thus the two inclusions are calculated as one inclusion in Table 4. Although the two objects are almost resolved for Case 14, when the inclusions are separated by 6.3 mm, the profiles of the two objects overlap and cannot be resolved using the FWHM as the threshold.

In contrast, TM-FT is able to reconstruct two separate objects for all cases, including the 1.4 mm separation case, and recover the correct size with a maximum error of 25%. For all cases, the error in the recovered fluorescence absorption is less than 11%. This experiment shows that TM-FT can resolve two objects separated by 1.4 mm, which is approximately equal to the size of the focal spot of the focused ultrasound and the distance between the line scans. Consequently, the spatial resolution limit for TM-FT relies on the focal spot size of the focused ultrasound. While choosing a focused ultrasound with a smaller focal spot will increase the spatial resolution, it will also require an increase in the number of scan lines, resulting in a longer scan time.

4. CONCLUSION

This experimental study investigates the performance of the TM-FT system using tissue-mimicking phantoms in resolving the concentration, size, and location of embedded fluorophore inclusions. The high scattering of light combined with the inherently limited spatial resolution of FT can be seen in the low spatial resolution and quantitative accuracy of the FT reconstructed absorption and concentration maps. In addition, the dependence on the source and detector configuration can also be seen from the lower resolution in the *y* direction and more specifically from phantom study 2. Depth dependence, as the quantitative accuracy and resolution of the ThermoDots inclusion, decreases as the inclusion is moved away from the center of the phantom. On the other hand, extensive phantom studies show that TM-FT provides superior spatial resolution and quantitative accuracy and does not depend on the geometry of the optical sources and detectors. TM-FT uses the thermo-sensitive quantum yield of the temperature-dependent ThermoDots and the localized heating from focused ultrasound to directly map the location and structure of the ThermoDots distribution with high spatial resolution. This information is used as *a priori* data and incorporated into the FT reconstruction program to provide high spatial resolution and quantitatively accurate images.

The spatial resolution study investigated the resolution limit of the TM-FT system. The spatial resolution is dependent on two factors: the focused ultrasound scanning pattern and the focal spot size. However, as the distance between the line scans is equal to the focal spot size, the resolution of TM-FT is ultimately determined by the focal spot size (~1.33 mm). Consequently, the focal spot size can be reduced by choosing a transducer with a smaller focal spot or by increasing the frequency. However, this will require additional line scans to cover the same area and will result in a longer data acquisition time. In addition, while increasing the frequency of the transducer will reduce the size of the focal spot, this will also lead to a decrease in the penetration depth [21].

For FT reconstructions, when using *structural a priori* information, the accuracy of this *a priori* information can be a source of error. Errors can occur when the fluorescence is not exactly aligned or confined uniformly within the specified region from anatomical imaging modalities, such as MRI, CT, or ultrasound, as it is assumed that the fluorophore distribution is homogenous within the defined region, such as a tumor boundary. However, this is not the case for TM-FT as it uses the temperature dependence of the fluorophore to provide high spatial resolution *functional a priori* that is not based on anatomical information. As TM-FT heavily depends on the accuracy of the fluorescence *a priori* binary map, it follows that this could be a source of error if the accuracy of the binary map is compromised. Regardless, the results show that this error is minimal compared to the improvement in size and quantitative accuracy of TM-FT. The error in ThermoDots fluorescence absorption recovered is at most 12% compared to conventional FT alone, which averaged an error above 90%.

TM-FT has many applications from preclinical small animal imaging to the clinical treatment of cancer. The future lies in targeting these ThermoDots to provide tumor-specific imaging. Optical devices have become one of the highest growth areas in preclinical imaging due in large part to their use in the development and assessment of new drugs for

pharmaceutical research [1]. As a small animal imaging device, TM-FT has the potential to provide *in vivo* fluorescence images with superior spatial resolution and sensitivity than commercial fluorescence systems. TM-FT is not only competitive with the spatial resolution of photoacoustic tomography (PAT) but has superior sensitivity as PAT has an inherent sensitivity to absorption and not the exogenous fluorescence contrast [12]. Future work includes expanding the current TM-FT prototype and adapting ThermoDots for *in vivo* animal imaging studies.

Acknowledgment.

This research is supported in part by NIH grants under the Ruth L. Kirschstein National Research Service Award, Fulbright visiting scholar (Nouizi) and by the UCI Eugene Cota-Robles Fellowship.

Funding. National Institutes of Health (NIH) (P30CA062203, 1F31CA171915–01A1, R01EB008716, R33 CA120175, SBIR HHSN261201300068C); UCI Eugene Cota-Robles Fellowship; Fulbright Commission (Visiting Scholar).

REFERENCES

1. Leblond F, Davis SC, Valdés PA, and Pogue BW, “Pre-clinical whole-body fluorescence imaging: review of instruments, methods and applications,” J. Photochem. Photobiol. B 98, 77–94 (2010). [PubMed: 20031443]
2. Wunder A, Tung C-H, Müller-Ladner U, Weissleder R, and Mahmood U, “In vivo imaging of protease activity in arthritis: a novel approach for monitoring treatment response,” Arthritis Rheum 50, 2459–2465 (2004). [PubMed: 15334458]
3. Corlu A, Choe R, Durduran T, Rosen MA, Schweiger M, Arridge SR, Schnall MD, and Yodh AG, “Three-dimensional in vivo fluorescence diffuse optical tomography of breast cancer in humans,” Opt. Express 15, 6696–6716 (2007). [PubMed: 19546980]
4. Ntziachristos V, “Fluorescence molecular imaging,” Annu. Rev. Biomed. Eng 8, 1–33 (2006). [PubMed: 16834550]
5. Gruber JD, Paliwal A, Ghadyani H, Maytin E, Hasan T, and Pogue B, “High-frequency ultrasound-guided fluorescence tomography of protoporphyrin IX in subcutaneous tumors,” in Biomedical Optics and 3-D Imaging (Optical Society of America, 2010), paper BMB5.
6. Lin Y, Barber WC, Iwanczyk JS, Roeck W, Nalcioglu O, and Gulsen G, “Quantitative fluorescence tomography using a combined trimodality FT/DOT/XCT system,” Opt. Express 18, 7835–7850 (2010). [PubMed: 20588625]
7. Davis SC, Pogue BW, Springett R, Leussler C, Mazurkewitz P, Tuttle SB, Gibbs-Strauss SL, Jiang SS, Dehghani H, and Paulsen KD, “Magnetic resonance-coupled fluorescence tomography scanner for molecular imaging of tissue,” Rev. Sci. Instrum 79, 064302 (2008). [PubMed: 18601421]
8. Hyde D, de Kleine R, MacLaurin SA, Miller E, Brooks DH, Krucker T, and Ntziachristos V, “Hybrid FMT-CT imaging of amyloid-β plaques in a murine Alzheimer’s disease model,” Neuroimage 44, 1304–1311 (2009). [PubMed: 19041402]
9. Davis SC, Dehghani H, Wang J, Jiang S, Pogue BW, and Paulsen KD, “Image-guided diffuse optical fluorescence tomography implemented with Laplacian-type regularization,” Opt. Express 15, 4066–4082 (2007). [PubMed: 19532650]
10. Nouizi F, Kwong TC, Cho J, Lin Y, Sampathkumaran U, and Gulsen G, “Implementation of a new scanning method for high-resolution fluorescence tomography using thermo-sensitive fluorescent agents,” Opt. Lett 40, 4991–4994 (2015). [PubMed: 26512501]
11. Yuan B, Uchiyama S, Liu Y, Nguyen KT, and Alexandrakis G, “High-resolution imaging in a deep turbid medium based on an ultrasound-switchable fluorescence technique,” Appl. Phys. Lett 101, 033703 (2012).
12. Lin Y, Bolisay L, Ghijsen M, Kwong TC, and Gulsen G, “Temperature-modulated fluorescence tomography in a turbid media,” Appl. Phys. Lett 100, 073702 (2012).

13. Lin Y, Kwong TC, Bolisay L, and Gulsen G, "Temperature-modulated fluorescence tomography based on both concentration and lifetime contrast," J. Biomed. Opt 17, 056007 (2012). [PubMed: 22612130]
14. Chen Y and Li X, "Thermo/pH-responsive and reversible NIR fluorescent probes for optical molecular imaging," in Biomedical Optics and 3-D Imaging, OSA Technical Digest (CD) (Optical Society of America, 2010), paper JMA105.
15. Kim TH, Chen Y, Mount CW, Gombotz WR, Li X, and Pun SH, "Evaluation of temperature-sensitive, Indocyanine green-encapsulating micelles for noninvasive near-infrared tumor imaging," Pharm. Res 27, 1900–1913 (2010). [PubMed: 20568000]
16. Lin Y, Nouizi F, Kwong TC, and Gulsen G, "Simulation-based evaluation of the resolution and quantitative accuracy of temperature-modulated fluorescence tomography," Appl. Opt 54, 7612–7621 (2015). [PubMed: 26368884]
17. Lin Y, Yan H, Nalcioglu O, and Gulsen G, "Quantitative fluorescence tomography with functional and structural a priori information," Appl. Opt 48, 1328–1336 (2009). [PubMed: 19252634]
18. Yalavarthy PK, Pogue BW, Dehghani H, Carpenter CM, Jiang S, and Paulsen KD, "Structural information within regularization matrices improves near infrared diffuse optical tomography," Opt. Express 15, 8043–8058 (2007). [PubMed: 19547132]
19. Kwong TC, Nouizi F, Sampathkumaran U, Zhu Y, Alam MM, and Gulsen G, "Activatable thermo-sensitive ICG encapsulated Pluronic nanocapsules for temperature sensitive fluorescence tomography," Proc. SPIE 9339, 93390C (2015).
20. Pogue BW, McBride T, Osterberg U, and Paulsen K, "Comparison of imaging geometries for diffuse optical tomography of tissue," Opt. Express 4, 270–286 (1999). [PubMed: 19396284]
21. Gail H, "Interventional oncology," in Interventional Oncology: A Practical Guide for the Interventional Radiologist, Mueller P and Adams A, eds. (Springer, 2012), pp. 51–63.

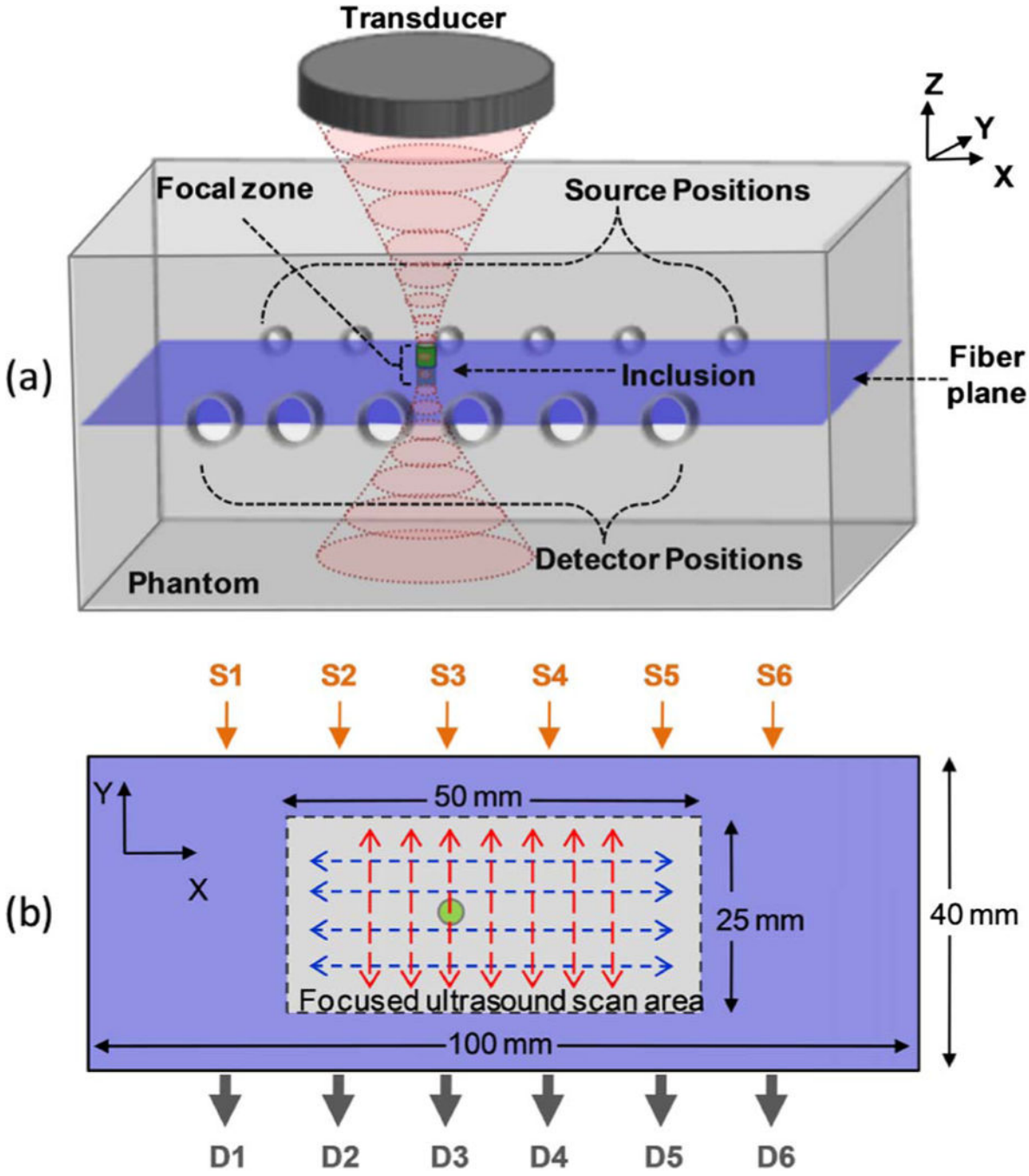

Fig. 1.

(a) Three-dimensional schematic of the phantom and focused ultrasound transducer. The transducer produces a focal zone of ~1.33 mm in diameter and 10 mm in length. The centers of the focal zone as well as the ThermoDots inclusion (green cylinder) are in the same plane (blue plane) as the source and detector optical fibers. (b) Cross-sectional view of the phantom at the fiber plane [blue plane in Fig. 1(a)] located 50 mm below the surface. The transducer is scanned over the focused ultrasound scan area (gray) in orthogonal directions forming the *x*-scan (blue dashed lines) and the *y*-scan (red dashed lines). Six source fibers (1

mm diameter, orange arrows) and six detector fibers (6 mm diameter, gray arrows) are positioned at opposite ends of the phantom for transillumination measurements.

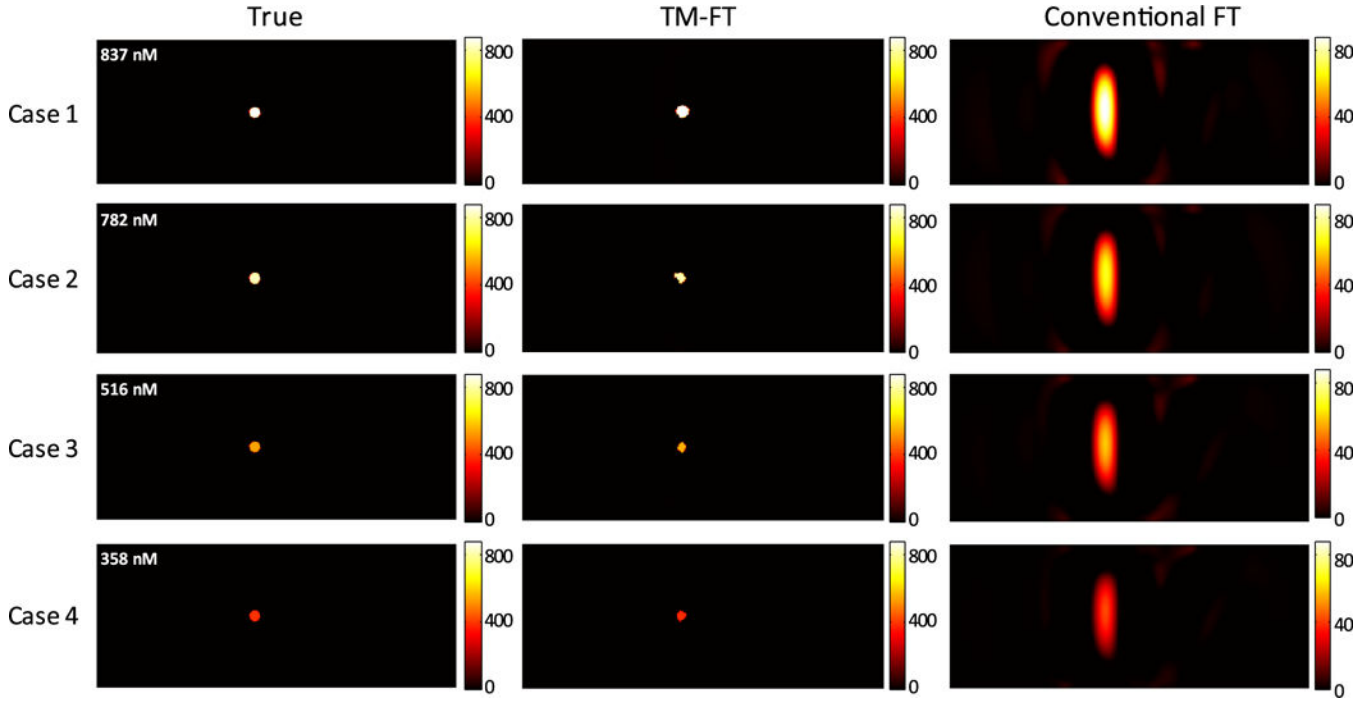

Fig. 2.

Reconstructed ThermoDots concentration maps comparing TM-FT (middle column) and conventional FT (right column) to the true value (left column) for four different ThermoDots concentrations. Case 1: 837 nM; Case 2: 782 nM; Case 3: 516 nM; and Case 4: 358 nM. The color bars all have units of nM.

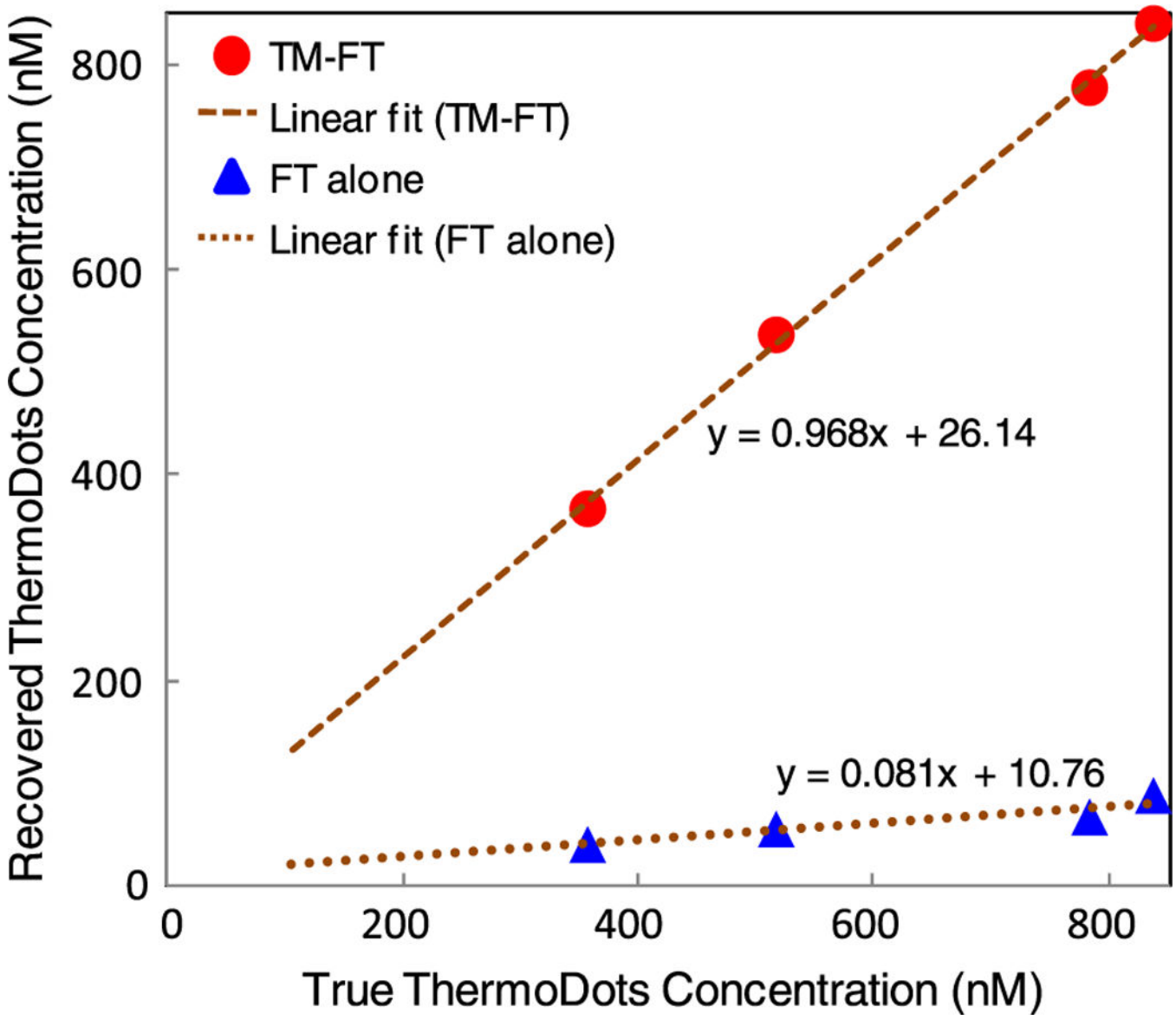

Fig. 3.

Plot of the recovered versus true ThermoDots concentrations. The red circles and blue triangles represent the recovered values with TM-FT and FT, respectively. The dashed and dotted lines represent the least squares linear fit for both cases. Although both TM-FT and FT alone show a linear response with respect to the true ThermoDots concentration, only TM-FT recovers the correct concentrations. The correlation coefficient for the TM-FT and stand-alone FT fitted curves is 0.998 and 0.863, respectively.

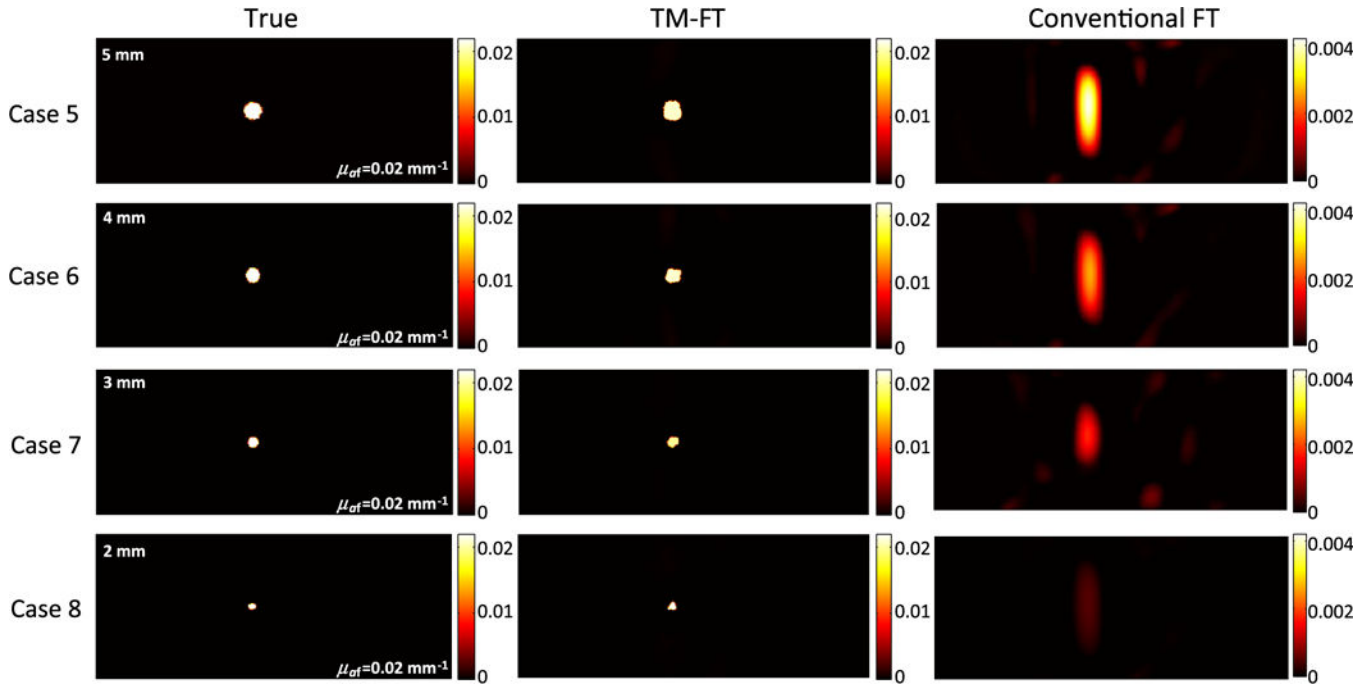

Fig. 4.

Reconstructed ThermoDots absorption maps comparing TM-FT (middle column) and conventional FT (right column) to the true values (left column) for the different sized inclusion diameters. Case 5: 5 mm; Case 6: 4 mm; Case 7: 3 mm; and Case 8: 2 mm. As seen in the images, the reconstructed absorption depends on the size of the inclusions for conventional FT. However, when the *functional a priori* is used for TM-FT, the true value can be reconstructed with less than 12% error for all cases. The color bars all have units of mm^{-1}.

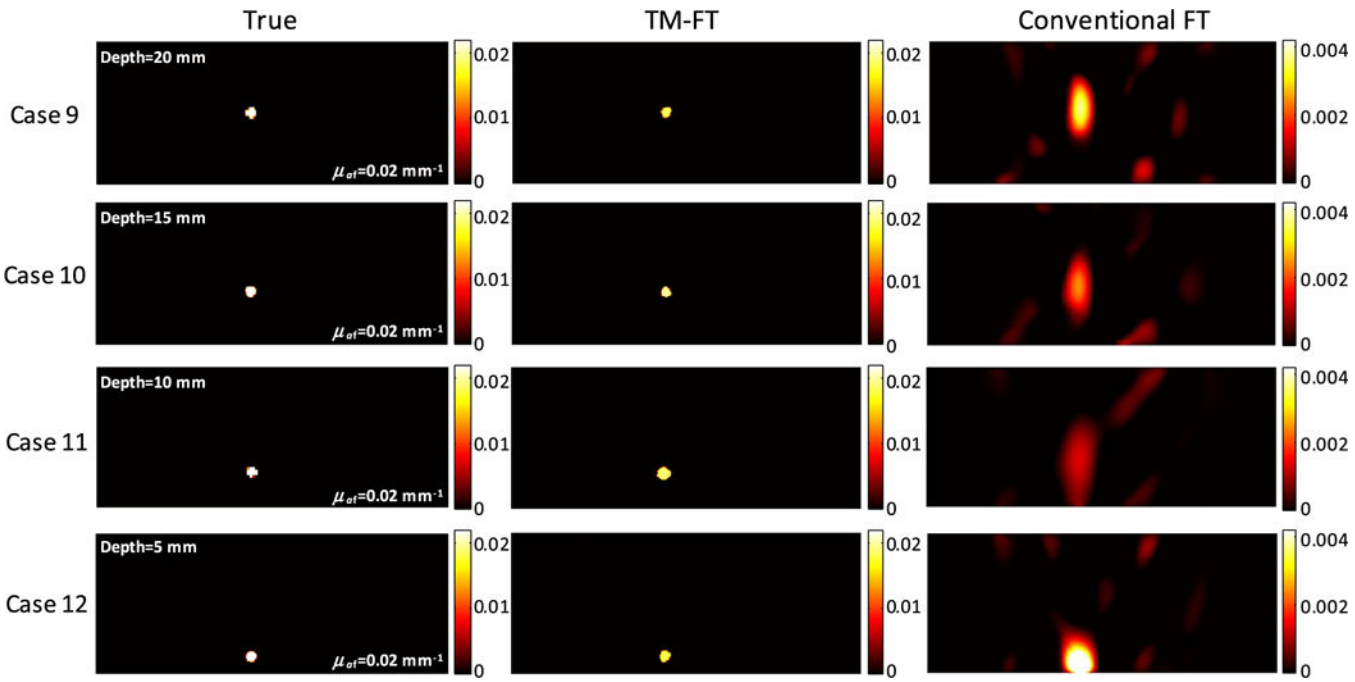

Fig. 5.

Reconstructed ThermoDots fluorescence absorption maps comparing TM-FT (middle column) and conventional FT (right column) to the true value (left column) for different ThermoDots inclusion depths. Case 9: 20 mm; Case 10: 15 mm; Case 11: 10 mm; and Case 12: 5 mm. The reconstructed fluorescence absorption depends on the depth. Conventional FT is unable to resolve the inclusion at 5 mm depth (Case 12). However, when the *functional a priori* is used for TM-FT, the true value can be reconstructed with less than 10.5% error for all cases. The color bars all have units of mm^{-1}.

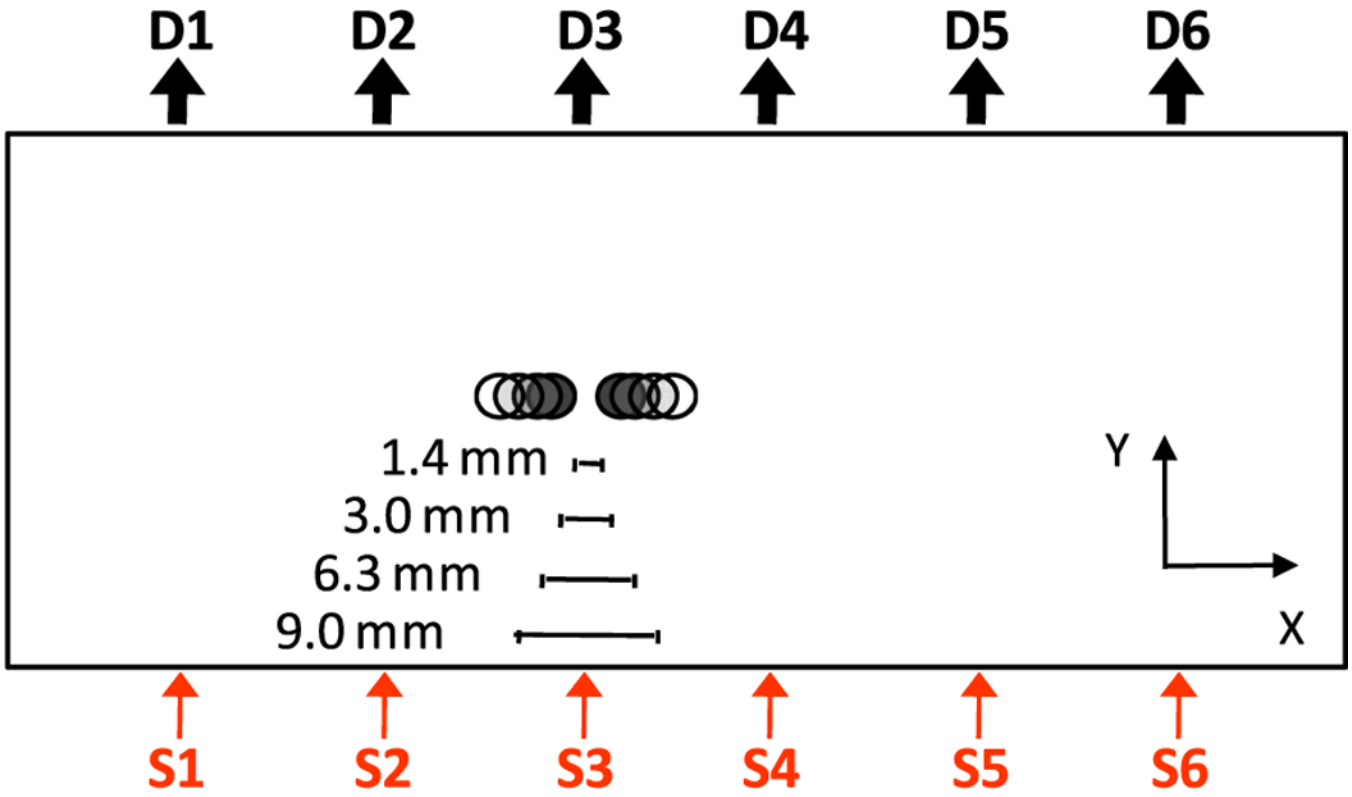

Fig. 6.

Experimental setup for phantom study 4: spatial resolution. Cross-sectional view of the phantom and ThermoDots inclusions separated by different distances.

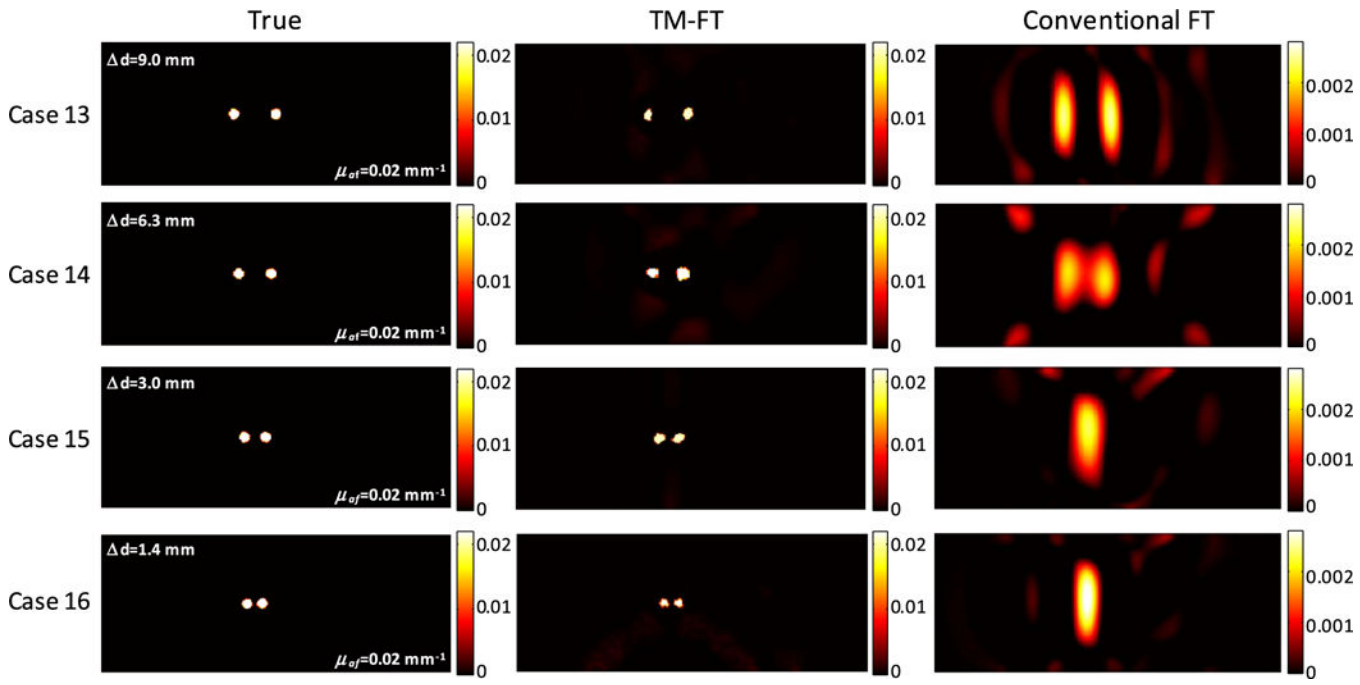

Fig. 7.

Reconstructed ThermoDots fluorescence absorption maps comparing TM-FT (middle column) and conventional FT (right column) to the true value (left column). **Δ***d* is the distance separation between the two objects. Case 13: 9 mm; Case 14: 6.3 mm; Case 15: 3 mm; and Case 16: 1.4 mm. Conventional FT is only able to fully separate the two objects for Case 13 when the separation distance is 9 mm. However, when the *functional a priori* is used for TM-FT, two separate objects can be seen for all four cases and the recovered ThermoDots fluorescence absorption is obtained with less than 11% error for all cases. The color bars all have units of mm^{-1}.

Table 1.

Recovered ThermoDots Concentration and Size of Inclusions with TM-FT and Conventional FT for Phantom Study 1: System Response Linearity

	True		TM-FT			Conventional FT		
Case	Concentration (nM)	FWHM (mm) *x*/*y*	Concentration (nM)	% Error Concentration	FWHM (mm) *x*/*y*	Concentration (nM)	% Error Concentration	FWHM (mm) *x*/*y*
1	836.5	3.00/3.00	838.2	0.2	3.00/3.25	86.9	89.6	5.75/19.25
2	782.4	3.00/3.00	777.1	0.7	2.50/3.00	65.0	97.7	5.75/19.25
3	516.0	3.00/3.00	536.2	3.9	2.25/2.50	55.5	89.2	5.50/18.25
4	357.9	3.00/3.00	366.3	2.3	2.75/2.75	39.4	89.0	5.00/18.00

Table 2.

Recovered ThermoDots Fluorescence Absorption and Size of Inclusions with TM-FT and Conventional FT for Phantom Study 2: Size Dependence

	True		TM-FT			Conventional FT		
Case	**μ_{af} (mm−1)**	**FWHM (mm) *x́ý***	**μ_{af} (mm−1)**	**% error μ_{af}**	**FWHM(mm) *x́ý***	**μ_{af} (mm−1)**	**% error μ_{af}**	**FWHM(mm) *x́ý***
5	0.0200	5.00/5.00	0.0190	5.1	5.00/5.25	0.0041	91.3	5.75/19.25
6	0.0200	4.00/4.00	0.0190	5.1	4.00/3.75	0.0026	94.4	5.75/19.00
7	0.0200	3.00/3.00	0.0198	1.2	3.25/3.25	0.0018	94.7	5.75/13.00
8	0.0200	2.00/2.00	0.0224	12.0	2.00/2.25	0.0007	96.8	5.25/20.25

Table 3.

Recovered ThermoDots Fluorescence Absorption and Size of Inclusions with TM-FT and Conventional FT for Phantom Study 3: Depth Dependence

	True			TM-FT			Conventional FT		
Case	**Depth (mm)**	**μ_{af} (mm−1)**	**FWHM (mm) *x́ý***	**μ_{af} (mm−1)**	**% Error μ_{af}**	**FWHM (mm) *x́ý***	**μ_{af} (mm−1)**	**% Error μ_{af}**	**FWHM (mm) *x́ý***
9	20	0.0200	3.00/3.00	0.0182	8.9	2.75/3.00	0.0018	91.3	5.75/13.25
10	15	0.0200	3.00/3.00	0.0199	0.8	3.00/3.00	0.0011	94.4	6.00/13.50
11	10	0.0200	3.00/3.00	0.0188	6.0	3.75/3.00	0.0007	94.7	7.25/21.75
12	5	0.0200	3.00/3.00	0.0180	10.2	3.00/3.00	Na	Na	Na

Table 4.

Recovered ThermoDots Fluorescence Absorption and Size of Inclusions with TM-FT and Conventional FT for Phantom Study 4: Spatial Resolution[a]

	True			TM-FT				FT			
Case	Δd (mm)	μ_{af} (mm−1)	FWHM (mm) x/y	μ_{af} (mm −1)	% Error μ_{af}	Left FWHM (mm) x/y	Right FWHM (mm) x/y	μ_{af} (mm −1)	% Error μ_{af}	Left FWHM (mm) x/y	Right FWHM (mm) x/y
13	9.0	0.02	3.00/3.00	0.0191	4.6	2.25/2.50	3.00/3.00	0.0025	87.6	5.00/17.75	5.00/18.25
14	6.3	0.02	3.00/3.00	0.0219	9.3	2.75/2.50	3.75/3.00	0.0020	90.0	17.25/14.25	17.25/13.25
15	3.0	0.02	3.00/3.00	0.0188	6.3	3.25/3.00	2.75/2.50	0.0022	88.8	7.50/17.50	7.50/18.00
16	1.4	0.02	3.00/3.00	0.0222	10.8	2.50/2.50	2.50/2.50	0.0015	92.6	5.50/18.50	5.50/17.50

[a] Δd is the distance separating the two objects.